Enhancing Nanofabrication at Scale via 3D Deconvolution Optimization

Hao-Chi Yen, and Qi Zhou

Abstract—Triplet-Triplet Annihilation Upconversion (TTA-UC) offers a unique avenue for achieving volumetric 3D printing at the micro- and nanoscale, holding promise across diverse fields like plasmonics, nanophotonics, and biomedicine. Distinguished from conventional two-photon absorption processes, TTA-UC can be initiated by low-power light sources yet retains the advantageous quadratic nature necessary for generating high-energy photons in spatially confined regions. This capability enables localized activation of polymerization reactions, positioning TTA-UC to transform the landscape of parallelized nanofabrication on a scalable basis. Nonetheless, to address the challenge of proximity effects arising from spatially overlapping light cones, this study delves into the exploration of advanced deconvolution algorithms with varied constraints. These efforts aim to achieve high-fidelity fabrication, marking a crucial step towards realizing the full potential of TTA-UC in modern manufacturing applications.

Index Terms—Upconversion, Nanofabrication, Scalability, 3D Deconvolution, Alternating Direction Method of Multipliers (ADMM)

1 Introduction and Background

THERE is exploding demand for fabricating complex three-dimensional (3D) structures with micro- and nanoscale features in a plethora of fields, ranging from nanooptics, nanophotonics, microfluidics, to biomedicine [1], [2], [3]. Some promising next-generation micro- and nanoprinting technologies for realizing such applications include dual-color polymerization [4] and light-sheet 3D laser microprinting [5]. These technologies leverage relatively low powered, continuous-wave lasers as the light source to parallelize the printing of millions of voxels (volume element in 3D) at one time. Nevertheless, these technologies rely on one-photon absorption (1PA) processes (**Fig. 1A**, on the left) and require the creation of precise light sheet optically, making them difficult to print structures with nanoscale resolution, and the scalability is really limited by the optics. Resultantly, one of the most well-established techniques for making nanoscale objects with arbitrary architectures is a volumetric 3D printing process with two-photon polymerization (2PP) [6], [7], [8], [9]. 2PP has been widely commercialized as a laboratory fabrication tool (Nanoscribe, UpNano, etc.). The quadratic nature of the two-photon absorption (2PA) (**Fig. 1A**, on the right) process enables precise spatial control of the polymerization process at a focal point down to nanoscale resolution in all dimensions. However, 2PA has a high threshold requirement; therefore, expensive, high-powered femtosecond pulsed lasers are required for 2PP, resulting in increased cost and reduced print speed to avoid undesired local heating effects. More importantly, it is practically impossible to parallelize the printing process (**Fig. 1B**) using 2PP due to the requisite high-power densities, making it extremely challenging to use this technology for mass production of 3D nanostructures.

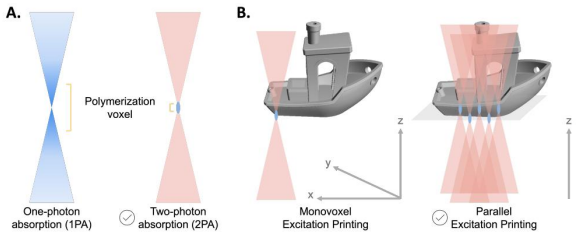

Fig. 1. (A) Comparison of one-photon absorption and two-photon absorption. (B) Comparison of monovoxel excitation printing and parallel excitation printing.

Triplet-triplet annihilation upconversion (TTA-UC) (**Fig. 2**) is a potential solution to this challenge as a net nonlinear process that can be triggered by low input powers [10], [11], [12], [13], [14], [15]. Materials that can facilitate TTA-UC convert two low energy photons into one higher energy photon by manipulating excitonic states in molecules. More specifically, sensitizers absorb low-energy photons, generate triplets via spin–orbit coupling, and transfer the triplet states to annihilators through triplet energy transfer. Two annihilator triplet states can then undergo triplet–triplet annihilation to generate one high-energy singlet excited state, which can radiatively decay and emit light at a higher energy than the incident photon energy. Intriguingly, the absorption steps involved in TTA-UC is linear, while the overall process is nonlinear (two photons in, one photon out). Thus, TTA-UC can be triggered by low power light sources, such as continuous-wave lasers or light-emitting diodes (LEDs). At the same time, it displays a quadratic nature/threshold behavior. Therefore, TTA-UC facilitated volumetric 3D printing can theoretically access nanoscale resolution (similar to 2PP in terms of resolution), while the

- *H. Yen is with the Department of Materials Science and Engineering and Electrical Engineering, Stanford University, Stanford, CA, 94305. E-mail: hcyen@stanford.edu*
- *Q. Zhou is with the Department of Electrical Engineering, Stanford University, Stanford, CA, 94305. E-mail: q69zhou@stanford.edu*

printing process can be easily parallelized and accelerated because of the low-power requirement (similar to dual-color polymerization and light-sheet 3D laser in terms of printing speed). Taken together, TTA-UC can provide exclusive possibilities for rapid, parallelized next-generation nanofabrication for wide-spanning applications.

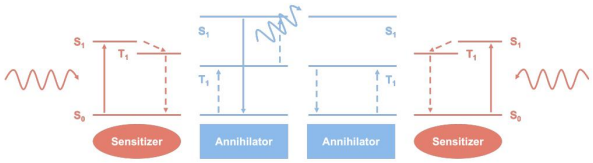

Fig. 2. Mechanism of triplet-triplet annihilation upconversion (TTA-UC).

2 Challenges and Related Work

In order to parallelize the printing, a digital micromirror device (DMD) (1920 × 1080 pixels, 7.56 µm micromirror pitch) is coupled to a high numerical aperture objective to project millions of voxels simultaneously. The magnification of the objective was chosen to be 20× so that the size of each pixel is already at the diffraction limit, while the projection image size is maximized to ensure the scalability of the technology. Meanwhile, a microstage, in sync with the DMD, is used to move the sample holder of the resin to achieve 3D printing. The setup of the optics and printing schema is summarized in **Fig. 3**. As an initial estimation, nanofabrication via TTA-UC is about two orders of magnitude faster than 2PP.

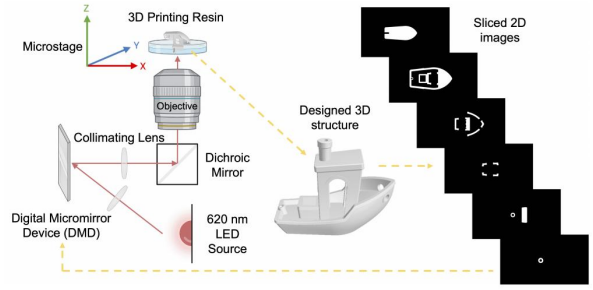

Fig. 3. Optics setup and printing workflow.

This nanofabrication method holds the promise of printing intricate 3D structures of arbitrary complexity. However, when projecting images that feature non-periodic and intricate shapes, the distribution of light across the focal plane becomes non-uniform due to the proximity effects of neighboring pixels. This phenomenon results in varying light intensity across the focal plane, with areas containing more activated pixels experiencing more intense light exposure while others receive less. This issue becomes particularly pronounced in the z-direction, leading to inconsistencies such as over-curing and under-curing within different regions of the printed objects. To address this, it becomes imperative to employ algorithms to correct the projected image, ensuring a nearly uniform distribution of light after optical processing. Previous attempts have utilized the Richardson-Lucy deconvolution method with notable improvements in feature fidelity, although further enhancements are still necessary [16]. Consequently, exploring more advanced deconvolution algorithms, such as half quadratic splitting (HQS) and the alternating direction method of multipliers (ADMM), each with unique constraints, presents a promising avenue for addressing this challenge effectively.

3 Methods

3.1 3D Simulation

Before diving into deconvolution, an optical kernel based on optics setup and a diffusion kernel based on materials properties were simulated as follows.

3.1.1 Optical Kernel

The optical kernel considers the spatial distribution of light intensity as a function of position, which is described by the equation:

$$I(x,y,z) = I_0 \exp\left(-\frac{2(x^2+y^2)}{w_0^2}\right) \exp\left(-\frac{2z^2}{w_z^2}\right) \exp(-\alpha c z)$$

where I is the light intensity at coordinates (x, y, z), I_0 is the initial light intensity at the focal point, w_0 is the beam waist radius in the transverse plane, w_z is the axial spread of the beam along the z-axis, α is the absorption coefficient of the medium, and c is the concentration of the absorbing species.

The optical kernel simulation provides the basis for understanding how light behaves when focused through the nanofabrication system's optics. The intensity $I(x, y, z)$ of light at any point is governed by the initial light intensity I_0 at the focal point, attenuating as it moves away from the center. The spread of the beam in the transverse plane is given by w_0 and along the axial direction by w_z, respectively. Additionally, the absorption of the medium, characterized by the absorption coefficient α and the concentration c of the absorbing species, also affects the intensity. The exponential terms describe the Gaussian nature of the beam profile in both the lateral and axial dimensions, while the term $\exp(-\alpha c z)$ accounts for the absorption of light by the medium. At last, I^2 is used to mimic the generation of the upconverted light triggered by the incident light. This simulation is crucial for predicting the actual light distribution within the resin during the printing process,

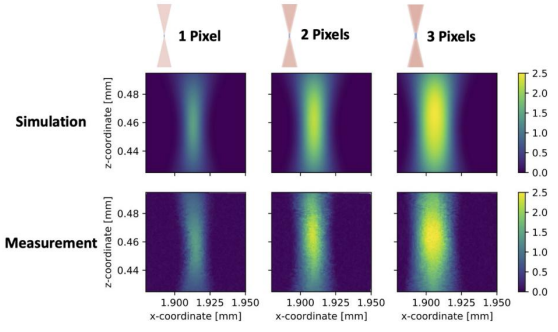

Fig. 4. Simulated versus real data visualization of the Point Spread Function (PSF) for the projections of different number of pixels, demonstrating the light intensity distribution in the x-z plane. Top row shows the simulation results, and the bottom row shows the actual data collected.

which directly impacts the resolution and quality of the nanofabricated structures.

Fig. 4 shown herein represents the Point Spread Function (PSF) for a singular pixel both simulated and captured through actual data measurements. The upper diagram depicts the theoretical intensity distribution of light as it interacts with the photopolymer, whereas the lower charts provide an empirical analysis across corresponding axes.

3.1.2 Diffusion Kernel

The diffusion kernel models radical diffusion within the material with respect to the incident light and is given by the equation:

$$K(r_d, t) = \frac{1}{(4\pi Dt)^{3/2}} \exp\left(-\frac{r_d^2}{4Dt}\right)$$

where K is the diffusion kernel, r_d is the radial distance for diffusion, t is the time step in the diffusion process, and D is the diffusion coefficient in the material.

The diffusion kernel captures the dynamics of the radicals generated by photoinitiator molecules and the resultant polymerization that occurs within the resin during the 3D printing process. Here, D represents the diffusion coefficient, d_t is the time step over which diffusion occurs, and r_d denotes the radial distance from the source of diffusion. The equation models the diffusion as a continuous process, described by a time-dependent Gaussian distribution. The $1/(4\pi Dd_t)^{3/2}$ term normalizes the distribution, ensuring the conservation of mass as the radicals spread out. The $\exp(-r_d^2/(4Dd_t))$ term describes how the radicals spread through the resin, affecting the curing process's uniformity and the eventual resolution of the printed structures.

3.1.3 3D convolution

This sequential approach—starting with the optical kernel then incorporating diffusion effects—provides a relatively comprehensive simulation of the 3D printing process. It can have precise adjustments based on the actual printing parameters to counteract uneven light distribution and diffusion-induced variations, ensuring the fabrication of high-fidelity nanostructures.

The Final Kernel, integrating both optical and diffusion effects previously modeled, is applied to the Benchy structure. Benchy is a benchmark structure in the field of 3D printing, since it features various challenging geometries such as overhangs, small details, curves, and flat surfaces. This step is aimed to simulate the intricate interplay of light with the material, mapped across Benchy's unique geometry. Through this convolution of the composite kernel with Benchy, it becomes possible to forecast how light scattering and molecule diffusion impact the nanoscale print. This predictive insight is crucial for adjusting printing parameters to achieve precise outcomes, highlighting the importance of the kernel in refining the printing process for accuracy and detail.

3.2 3D Deconvolution

3.2.1 Richardson-Lucy Deconvolution

The Richardson-Lucy (RL) deconvolution is an iterative algorithm designed for image restoration, particularly effective in scenarios where the point spread function (PSF) (the final kernel in this case) is known. The essence of RL deconvolution lies in its iterative process, aiming to recover the original image by minimizing the differences between observed images and the convolution of the estimated images with the PSF.

$$\hat{u}^{(t+1)} = \hat{u}^{(t)} \cdot \left(\frac{d}{\hat{u}^{(t)} \otimes P} \otimes P^*\right)$$

By applying RL deconvolution, it is possible to correct optical aberrations and improve the precision of the fabrication process. This adjustment is vital for applications requiring high-resolution and -fidelity nanostructures, such as in photonics and biomedicine, where even minor inaccuracies can significantly impact the functionality and efficiency of the fabricated devices.

The implementation of RL deconvolution in the context of 3D nanofabrication involves adjusting the light intensity distribution to achieve uniform polymerization across the printing plane. This correction process is essential for overcoming the challenges posed by uneven light distribution, ensuring that each voxel within the printed structure is accurately cured, thereby avoiding issues like over-curing or under-curing. The ability of RL deconvolution to iteratively refine the light intensity map makes it an invaluable tool in the pursuit of high-precision nanofabrication. As a preliminary result, RL deconvolution was applied to Benchy structure and promoted better prints as shown in **Fig. 5** but still need significant efforts or improvement to achieve desired Bency.

3.2.2 Alternative Direction Method of Multiplier

The Alternative Direction Method of Multipliers (ADMM) [17] is a powerful optimization algorithm that breaks down complex problems into simpler subproblems, solving them iteratively to find an optimal solution efficiently. This method is particularly effective in scenarios involving constraints, as it alternates between optimizing different components of the objective function while ensuring that these components adhere to a set of constraints.

The deconvolution problem can be defined as follows:

$$\min_x f(x) + g(z)$$
$$\text{subject to } Kx - z = 0$$
$$\text{where } f(x) = \frac{1}{2}\|Ax - b\|_2^2, \text{ and } g(z) = I_{R_+}(z),$$
$$K_{Nn} = \begin{bmatrix} I \end{bmatrix}, \quad K_{TV} = \begin{bmatrix} D_x \\ D_y \\ D_z \end{bmatrix}, \quad K_{TV,Nn} = \begin{bmatrix} I \\ D_x \\ D_y \\ D_z \end{bmatrix}$$

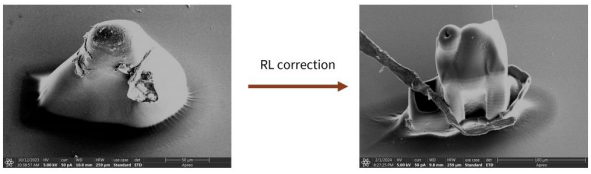

Fig. 5. Enhancement in edge sharpness and detail resolution observed in printed Benchy structures when applying 3D RL deconvolution.

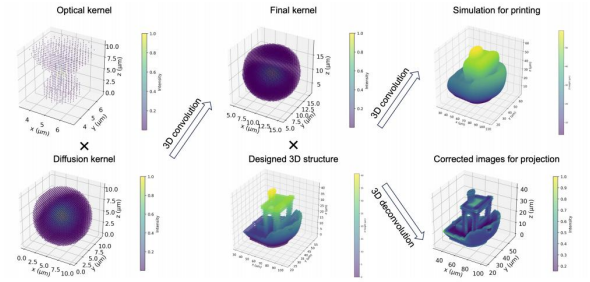

Fig. 6. The process of 3D convolution to simulate the light-intensity distribution in TTA-UC printing and subsequent deconvolution to correct light dosage

The objective function described,

$$\min_{x,z} \; f(x) + g(z),$$

underscores the dual nature of the problem ADMM addresses. Here, $f(x)$ represents one aspect of the objective, such as the fidelity of the reconstruction to the observed data, encapsulated by

$$\frac{1}{2} \|Ax - b\|_2^2 ,$$

where A is a linear operator, i.e., convolution operation in this case, x is the variable representing the estimated image, and b is the observed (blurred and noisy) image. On the other hand, $g(z)$ embodies regularization terms that impose certain desired properties on the solution, like sparsity or non-negativity or total variation. The inclusion of $g(z) = I_{R_+(z)}$ introduces nonnegativity (Nn) regularization terms to the optimization.

The Total Variation (TV) prior, denoted in the context of ADMM as TV, is instrumental in promoting sparsity in the gradient of the image. This means it encourages the image to have fewer and simpler transitions, which is especially beneficial in enhancing edge definition and reducing noise. In the realm of nanofabrication, applying the TV prior helps in preserving the sharpness and clarity of nanostructures' boundaries, ensuring that even at the nanoscale, fabricated structures are defined accurately.

The Nonnegativity prior Nn ensures that the solution z, and by extension the estimated image x, contains no negative values. This constraint is naturally aligned with physical realities in nanofabrication, where negative values for parameters such as light intensity or material density do not make sense. Enforcing nonnegativity helps in maintaining the physical plausibility of the deconvolved image, which is crucial for accurately guiding the fabrication process.

The constraints,

$$Kx - z = 0,$$

facilitate the coupling of the two parts of the objective function, allowing ADMM to efficiently find a balance between them. This balance is crucial in nanofabrication, where the goal is to achieve high-fidelity fabrication that accurately reflects the intended design. **Fig. 6** summarizes the methodology of the entire process from simulation to deconvolution.

4 Experimental Results

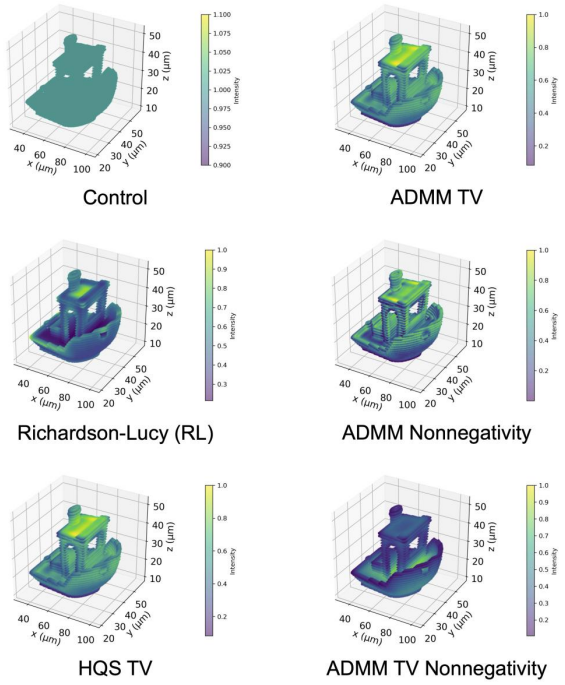

Fig. 7. Visualization of 3D-deconvolved Benchy of different deconvolution algorithms with various constraints.

The results of 3D deconvolution using different algorithms and constraints are presented in **Fig. 7**. It is evident that half quadratic splitting (HQS) with TV and ADMM with TV converge to similar solutions. Utilizing ADMM with non-negativity constraints yields the lowest loss, as defined by the mean square error of $Ax - b$, particularly outperforming RL. This improvement can be attributed to the advantages of the ADMM algorithm in finding optimal solutions, and the non-negativity constraint inherently aligns with the physical process of 3D printing, where negative light intensity or material deposition is nonexistent [18], [19]. By enforcing non-negativity, the deconvolution process prohibits the generation of physically implausible corrections to the light intensity map, ensuring a more accurate and faithful replication of the desired nanostructures.

When simultaneously adding TV and non-negativity constraints, competing objectives arise. TV constraints aim to minimize variation between adjacent elements (e.g., pixels in image processing), promoting smoothness or sparsity. Non-negativity constraints, on the other hand, ensure that values do not drop below zero. When an algorithm attempts to satisfy both constraints, especially in regions where the optimal solution requires fine balance, it can lead to large updates as the optimizer oscillates between meeting one constraint and then the other. This might explain why, with both non-negativity and TV constraints, the loss over iterations initially reaches a lower point but then explodes.

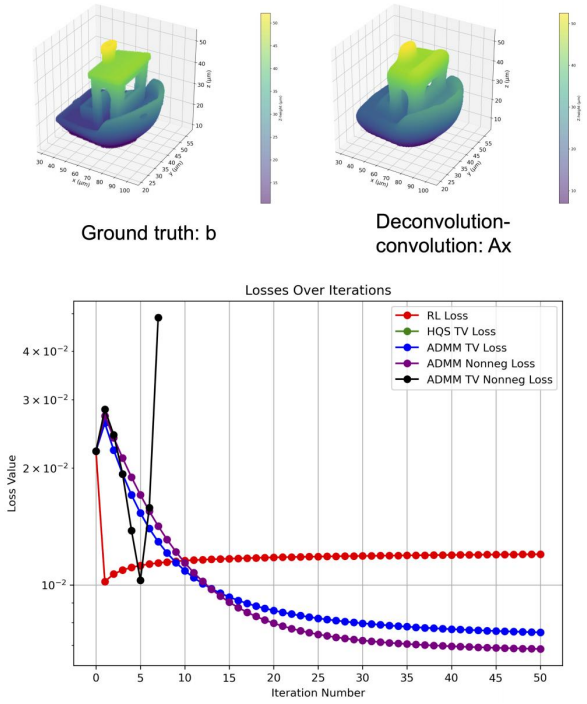

Fig. 8. Losses over iterations of different deconvolution algorithms with various constraints.

5 Conclusion

The implementation of ADMM in nanofabrication marks a significant stride towards achieving scalable, high-fidelity manufacturing of nanostructures. By harnessing ADMM, researchers and engineers can transcend traditional limitations, opening pathways for advanced applications across diverse fields, from photonics to biomedicine, where precise and scalable fabrication of nanostructures is imperative. For instance, in photonics, this enhanced fabrication technique holds the potential to foster the development of more efficient light-manipulating metasurfaces, while in biomedicine, it could facilitate the creation of more precise microfluidic devices.

Looking forward, 3D micro- and nanoscale fabrication using TTA-UC along with deconcolution optimization holds the promise to revolutionize fabrication in terms of both speed and resolution, rendering it suitable for the industrial production of large-scale, precisely tailored micro- and nanopatterned materials. Moreover, the printing resin can be further developed to accommodate other materials such as glass and ceramics, and can be fine-tuned to incorporate additional desired functionalities, including biocompatibility for chemical and biological applications. In essence, this technology harbors immense potential for applications ranging from constructing metasurfaces for AR/VR purposes to fabricating cell scaffolds for tissue engineering, large-scale production of hydrophobic surfaces, and even the development of photonic integrated circuits, among others.

Acknowledgments

The authors would like to thank Qingqing Zhao and Prof. Gordon Wetzstein for providing great insight on this work.

References

[1] J. Bauer, C. Crook, and T. Baldacchini, "A sinterless, low-temperature route to 3d print nanoscale optical-grade glass," *Science*, vol. 380, no. 6648, pp. 960–966, 2023.
[2] A. K. Nguyen and R. J. Narayan, "Two-photon polymerization for biological applications," *Materials Today*, vol. 20, pp. 314–322, 2017.
[3] J. L. Sanchez Noriega *et al.*, "Spatially and optically tailored 3d printing for highly miniaturized and integrated microfluidics," *Nature Communications*, vol. 12, no. 1, pp. 1–13, 2021.
[4] M. Regehly *et al.*, "Xolography for linear volumetric 3d printing," *Nature*, vol. 588, no. 7839, pp. 620–624, 2020.
[5] V. Hahn *et al.*, "Light-sheet 3d microprinting via two-colour two-step absorption," *Nature Photonics*, pp. 1–8, 2022.
[6] S. Koo, "Advanced micro-actuator/robot fabrication using ultra-fast laser direct writing and its remote control," *Applied Sciences*, vol. 10, p. 8563, 2020.
[7] Q. Geng, D. Wang, P. Chen, and S. C. Chen, "Ultrafast multi-focus 3-d nano-fabrication based on two-photon polymerization," *Nature Communications*, vol. 10, no. 1, pp. 1–7, 2019.
[8] L. Zheng *et al.*, "Nanofabrication of high-resolution periodic structures with a gap size below 100 nm by two-photon polymerization," *Nanoscale Res Lett*, vol. 14, pp. 1–9, 2019.
[9] Z. Faraji Rad, P. D. Prewett, and G. J. Davies, "High-resolution two-photon polymerization: the most versatile technique for the fabrication of microneedle arrays," *Microsystems & Nanoengineering*, vol. 7, no. 1, pp. 1–17, 2021.
[10] S. N. Sanders *et al.*, "Triplet fusion upconversion nanocapsules for volumetric 3d printing," *Nature*, vol. 604, no. 7906, pp. 474–478, 2022.
[11] D. K. Limberg, J. H. Kang, and R. C. Hayward, "Triplet-triplet annihilation photopolymerization for high-resolution 3d printing," *J Am Chem Soc*, vol. 144, pp. 5226–5232, 2022.
[12] Z. Wang, Y. Zhang, Y. Su, C. Zhang, and C. Wang, "Three-dimensional direct-writing via photopolymerization based on triplet—triplet annihilation," *Science China Chemistry*, vol. 65, no. 11, pp. 2283–2289, 2022.
[13] Z. Wang, Y. Hou, Z. Huo, Q. Liu, W. Xu, and J. Zhao, "Spatially confined photoexcitation with triplet–triplet annihilation upconversion," *Chemical Communications*, vol. 57, no. 72, pp. 9044–9047, 2021.
[14] Z. Luo, D. Wang, K. Li, D. Zhong, L. Xue, Z. Gan, and C. Xie, "Three-dimensional nanolithography with visible continuous wave laser through triplet up-conversion," *The Journal of Physical Chemistry Letters*, vol. 14, no. 3, pp. 709–715, 2023.
[15] V. Hahn, N. M. Bojanowski, P. Rietz, F. Feist, M. Kozlowska, W. Wenzel, E. Blasco, S. Brase, C. Barner-Kowollik, and M. Wegener, "Challenges and opportunities in 3d laser printing based on (1+ 1)-photon absorption," *ACS Photonics*, vol. 10, no. 1, pp. 24–33, 2022.
[16] A. Orth, D. Webber, Y. Zhang, K. L. Sampson, H. W. de Haan, T. Lacelle, R. Lam, D. Solis, S. Dayanandan, T. Waddell *et al.*, "Deconvolution volumetric additive manufacturing," *Nature Communications*, vol. 14, no. 1, p. 4412, 2023.
[17] S. Boyd, N. Parikh, E. Chu, B. Peleato, J. Eckstein *et al.*, "Distributed optimization and statistical learning via the alternating direction method of multipliers," *Foundations and Trends® in Machine learning*, vol. 3, no. 1, pp. 1–122, 2011.
[18] Y. Xu, Y. Sun, H. Wu, W. Cao, L. Bai, S. Tao, Z. Tian, Y. Cui, X. Hao, C. Kuang *et al.*, "Regularized deconvolution for structured illumination microscopy via accelerated linearized admm," *Optics & Laser Technology*, vol. 169, p. 110119, 2024.
[19] J. M. Long, J. Y. Chun, and T. K. Gaylord, "Admm approach for efficient iterative tomographic deconvolution reconstruction of 3d quantitative phase images," *Applied Optics*, vol. 60, no. 27, pp. 8485–8492, 2021.